Supporting Information

Harnessing A New Co-Host System and Low Concentration of New TADF Emitters Equipped with Trifluoromethyl and Cyano Substituted Benzene as Core for High Efficiency Blue OLEDs

Chih-Lun Yi,[1] Chang-Lun Ko, [2] Tzu-Chin Yeh,[1] Chih-Yang Chen,[2] Yi-Sheng Chen[1], Deng-Gao Chen[1], Pi-Tai Chou,[1] Wen-Yi Hung,[2,3]*, Ken-Tsung Wong[1,4]*

[1] Department of Chemistry, National Taiwan University, Taipei 106, Taiwan

[2] Department of Optoelectronics and Materials Technology, National Taiwan Ocean University, Keelung 202, Taiwan

[3] Center of Excellence for Ocean Engineering, National Taiwan Ocean University, Keelung, 202, Taiwan

[4] Institute of Atomic and Molecular Science, Academia Sinica, Taipei 10617, Taiwan

Corresponding Authors W.-Y. Hung (wenhung@mail.ntou.edu.tw), K.-T. Wong (kenwong@ntu.edu.tw).

Contents		Page

General Information

All chemicals and reagents were used as received from commercial sources without purification. Solvents for chemical synthesis were purified by distillation. All chemical reactions were carried out under an argon or nitrogen atmosphere.

Thermal Properties

Thermogravimetric analysis (TGA) was undertaken with a TGA Q500 instrument. The thermal stability of the samples under a nitrogen atmosphere was determined by measuring their 5% weight loss while heating at a rate of 10 ^{o}C min^{-1}. Differential scanning calorimetry (DSC) analyses were performed on a TA Instrument DSC-2920 Low Temperature Difference Scanning Calorimeter at a heating rate of 10 ^{o}C min^{-1} under nitrogen.

Cyclic voltammetry

The electrochemical properties of all the products were measured by cyclic voltammetry by using a CHI619B potentiostat. The oxidation potential was determined by cyclic voltammetry using 0.1M *n*-Bu_4NPF_6 ($TBAPF_6$) in CH_2Cl_2 as a supporting electrolyte and a scan rate of 100 mV s^{-1}. The reduction potential was recorded using 0.1M *n*-Bu_4NClO_4 (TBAP) in DMF as a supporting electrolyte and a scan rate of 100 mV s^{-1}. A standard 3-electrode cell comprising silver/silver chloride (Ag/AgCl), a platinum wire and a glassy carbon electrode as the reference, counter, and working electrodes, respectively, were used. All potentials were recorded versus Ag/AgCl (saturated) as a reference electrode. Oxidation of the ferrocene/ferrocenium (Fc/Fc^+) redox couple in $CH_2Cl_2/TBAPF_6$ occurs at E'_o = + 0.47 V and reduction of the ferrocene/ferrocenium (Fc/Fc^+) redox couple in DMF/TBAP occurs at E'_o = + 0.51 V vs. Ag/AgCl (saturated). HOMO and LUMO levels were calculated from the oxidation / reduction half-wave

potential with the formula: E_{HOMO} = -4.8 – (E_{onset}^{oxi} – $E^{Fc/Fc+}$) (eV) and E_{LUMO} = -4.8 – (E_{onset}^{red} – $E^{Fc/Fc+}$) (eV).

Photophysical measurements

Photophysical characteristics of compounds in solutions were collected at room temperature by using 10^{-5} M dichloromethane (CH_2Cl_2) solutions of all compounds, which were carefully purged with nitrogen prior to measurements. UV-visible absorption spectra were recorded on a spectrophotometer (HITACHI U2800A). PL spectra were measured with a fluorescence spectrophotometer (HITACHI F9500). Phos spectra were measured with a fluorescence spectrophotometer (HORIBA Fluoromax-4P) with cryogenic system. Quantum efficiency measurements were recorded with an integration sphere (HORIBA Quanta-ϕ) coupled with a fluorometer (HORIBA Fluoromax-4P), which gave anthracene a quantum yield of 23%. The excitation wavelength at PL, phosphorescence, and PLQY measurement is based on the absorption peak of compound. The time-resolved studies were performed using a time-correlated single photon counting (TCSPC) S-4 system (TimeHarp 260, PicoQuant) with the pulse LED at 285 nm (PLS280, PicoQuant) as the photoexcitation light source. The emission decays were fitted by the sum of exponential functions with a temporal resolution of ~300 ps via the deconvolution of instrument response function. The charging voltage of the ICCD was open at various delay times with an adjustable gated window synchronized with the firing time of the excitation pulse. In this study, the third harmonic (355 nm, fwhm ~8 ns) of an Nd:YAG laser (Continuum Surelite) was used as the excitation pulse.

Computational Method

All the theoretical calculation was performed in the gaseous state using Gaussian

09_E01 program package through Taiwania 1 built by the National Applied Research Laboratories, Taiwan. The S_0 geometries of all TADF molecules were optimized at a B3LYP/6-31G(d) level with density functional theory (DFT). The S_1 and T_1 geometries were optimized at M06-2x/6-31G(d) level with time-dependent density functional theory (TD-DFT).

Time-of-flight (TOF) mobility measurements

In charge-transport properties of SimCP and *o*CF_3-T2T, we used the time-of-flight (TOF) transient photocurrent technique. The TOF device was configured as: ITO glass/ compound/Ag (150 nm), which were then placed inside a cryostat and kept under vacuum. The thickness of organic film was monitored in situ with a quartz sensor and calibrated by a thin film thickness measurement (K-MAC ST2000). A pulsed nitrogen laser (337 nm) was used as the excitation light source through the transparent electrode (ITO) inducing photogeneration of a thin sheet of excess carriers. Under an applied dc bias, the transient photocurrent was swept across the bulk of the organic film toward the collection electrode (Ag), and then recorded with a digital storage oscilloscope. Depending on the polarity of the applied bias, selected carriers (holes or electrons) are swept across the sample with a transit time of t_T. With the applied bias V and the sample thickness D, the applied electric field $E = V/D$, and the carrier mobility is then given by $\mu = D/(t_T\ E) = D^2/(Vt_T)$, in which the carrier transit time, t_T, can be extracted from the intersection of two asymptotes to the tail and plateau sections in the double-logarithmic plots.

OLED Device Fabrications

All chemicals were purified through vacuum sublimation prior to use. The OLEDs were fabricated through vacuum deposition of the materials at 10^{-6} Torr onto the ITO-

coated glass substrates having a sheet resistance of 15 Ω sq^{-1}. Prior to use the ITO surface was cleaned ultrasonically; i.e. with acetone, methanol, and deionized water in sequence and finally with UV-ozone. The deposition rate of each organic material was ca. 1–2 Å s^{-1}. The *J–V–L* characteristics of the devices were measured simultaneously in a glove-box using a Keithley 6430 source meter and a Keithley 6487 picoammeter equipped with a calibration Si-photodiode. EL spectra were measured using a photodiode array (Ocean Optics USB2000+).

Measurement and Simulation of Angle-Dependent PL Spectra:

The angular dependent *p*-polarized fluorescence intensity was measured in an attempt to analyze the transition dipole moment of emitters. The experimental setup was similar to that described in literature[1], which composed of a motorized rotation stage, a fused silica-based half-cylindrical len, a longpass filter to stop the excitation beam, a polarizer, and a fiber-guided spectrometer (Ocean Optics USB4000) to collect the polarized emission. A continuous-wave Nd:YAG laser (355 nm, 10 kHz) was used as the excitation source which was fixed at an incident angle of 45°. The sample was deposited on top of a quartz substrate and encapsulated under N_2 atmosphere. Intensity of the *p*-polarized emission was recorded from 0° to 90° in steps of 5°. The data were analyzed using SETFOS 4.5 (Fluxim AG, Switzerland) to fit the ratio of horizontal dipoles (Θ). A completely random orientation in tris-(8-hydroxyquinoline)aluminum (Alq3) with Θ = 0.66 was employed for system calibration. The refractive index *n* and extinction coefficient k in thin films were determined by ellipsometry (J. A. Woollam α-SE) and analyzed using Woollam CompleteEASE software.

[1] a) J. Frischeisen, D. Yokoyama, C. Adachi, W. Brütting, *Appl. Phys. Lett.* **2010**, *96*, 073302; b) S.-Y. Kim, W.-I. Jeong, C. Mayr, Y.-S. Park, K.-H. Kim, J.-H. Lee, C.-K. Moon, W. Brütting, J.-J. Kim, *Adv. Funct. Mater.* **2013**, *23*, 3896; c) A. Senes, S. C. J. Meskers, W. M. Dijkstra, J. J. van Franeker, S. Altazin, J. S. Wilson, R. A. J. Janssen, *J. Mater. Chem. C* **2016**, *4*, 6302.

Synthetic methods:

Synthesis of 2,4,6-trifluoro-3-iodo-5-(trifluoromethyl)benzonitrile (3).

1,3,5-trifluoro-2,4-diiodo-6-(trifluoromethyl)benzene (0.9 g, 2.0 mmol), CuCN (0.18 g, 2.0 mmol) and stir bar were mixed in 25 mL two-neck bottle. Under argon atmosphere, 5 mL NMP was added. The reaction was heated at 120 ^{o}C overnight. After cooling to room temperature, the reaction was directly filtered through celite then washed with dichloromethane and concentrated to give the crude product which was then purified by column chromatography (SiO_2, CH_2Cl_2/Hexane = 1/2) to provide compound **3** as a white solid (0.231 g, 33%). ^{19}F NMR (376 MHz, $CDCl_3$): δ = -56.97 (t, *J* = 22.6 Hz, 1 F), -74.84 (dd, *J* = 9.5, 3.2 Hz, 1 F), -75.83 – -76.13 (m, 1 F), -100.96 – -101.39 (m, 1 F). ^{13}C NMR (101 MHz, $CDCl_3$): δ = 68.5, 68.6, 68.8, 68.9, 69.1, 69.2, 91.2, 91.4, 91.6, 106.8, 116.1, 118.8, 121.5, 124.3, 160.5, 160.6, 160.6, 161.7, 161.8, 161.9, 163.2, 163.3, 163.4, 164.0, 164.1, 164.1, 164.4, 164.4, 164.5, 166.6, 166.7, 166.8.

Synthesis of 9,9',9''-(2,4-diiodo-6-(trifluoromethyl)benzene-1,3,5-triyl)tris(9*H*-carbazole) (4).

60% NaH (0.87 g, 21.75 mmol) was added to a stired solution of carbazole (3.2 g, 19.14 mmol) in DMF (40 mL) under an argon atmosphere at room temperature and then stirred for 30 min. A solution of compound **2** (2.62 g, 5.8 mmol) in DMF (18 mL) was added into reaction mixture and stirred at room temperature overnight. The reaction was poured into water and white powder appeared. After filtered and washed with ethanol and then reprecipitated from CH_2Cl_2/ MeOH to provide compound **4** as a white solid (3.53 g, 67%). ^{1}H NMR (400 MHz, CD_2Cl_2): δ = 7.14 (d, *J* = 8.0 Hz, 2 H), 7.20 (d, *J* = 8.0 Hz, 4 H), 7.35-7.40 (m, 6 H), 7.51-7.59 (m, 6 H), 8.17 (t, *J* = 7.4 Hz, 6 H); ^{19}F NMR (100 MHz, CD_2Cl_2): δ = -59.50 (s, 3 F); ^{13}C NMR (100 MHz, CD_2Cl_2): δ = 110.0, 110.1, 113.5, 121.3, 121.5, 121.7, 122.6, 124.3, 124.4, 127.3, 138.5, 141.0, 142.6, 151.2.

HRMS (m/z, MALDI) calcd. for $C_{43}H_{24}F_3I_2N_3$ 893.0012 found 893.0022.

Synthesis of 2,3,4,6-tetra(9*H*-carbazol-9-yl)-5-(trifluoromethyl)benzonitrile (4CzIPN-CF_3).

Cs_2CO_3 (6.0 g, 18.4 mmol) was added to a stired solution of carbazole (2.77 g, 16.56 mmol) in DMSO (15 mL) under an argon atmosphere at room temperature and then stirred for 30 min. A solution of compound **3** (1,29 g, 3.68 mmol) in DMSO (5 mL) was added into reaction mixture and heated at 140 ^oC for 20 hr. After cooling to room temperature, the reaction was poured into water and yellow powder appeared, followed by filtered and washed with ethanol to give the crude product which was then purified by column chromatography (SiO_2, CH_2Cl_2/ Hexane = 1/1) to provide **4CzIPN-CF_3** as a yellow powder (1.47 g, 48%). ^1H NMR (400 MHz, CD_2Cl_2): δ = 6.68 (td, *J* = 1.4, 8.4 Hz, 2 H), 6.83 (t, *J* = 7.6 Hz, 2 H), 6.93 (d, *J* = 8.0 Hz, 2 H), 7.08-7.15 (m, 8 H), 7.23-7.26 (m, 4 H), 7.35 (d, *J* = 7.6 Hz, 2 H), 7.51 (t, *J* = 7.4 Hz, 2 H), 7.65 (d, *J* = 7.6 Hz, 2 H), 7.73-7.78 (m, 6 H), 8.27 (d, *J* = 8.0 Hz, 2 H); ^{19}F NMR (100 MHz, CD_2Cl_2): δ = -60.34 (s, 3 F); ^{13}C NMR (100 MHz, CD_2Cl_2): δ = 110.1, 110.4, 110.5, 110.6, 112.1, 120.0, 120.6, 120.9, 121.3, 121.6, 121.8, 122.3, 123.5, 124.2, 124.5, 124.8, 125.0, 125.1, 126.2, 126.3, 127.6, 138.2, 139.0, 139.2, 140.4, 142.2, 142.5, 145.5.; HRMS (FAB^+, m/z) calcd. for $C_{56}H_{32}F_3N_5$ 831.2610, found 831.2638.

Synthesis of 2,4,6-tri(9*H*-carbazol-9-yl)-3-(trifluoromethyl)benzonitrile (3CzIPN-H-CF_3).

Compound **4** (0.894 g, 1.0 mmol), CuCN (0.19 g, 2.1 mmol) and stir bar were mixed in 25 mL two-neck bottle. Under argon atmosphere, 10 mL NMP was added. The reaction was heated at 170 ^oC overnight. After cooling to room temperature, the reaction was directly filtered through celite then washed with dichloromethane and concentrated

to give the crude product which was then purified by column chromatography (SiO_2, CH_2Cl_2/ Hexane = 1/1) to provide **3CzIPN-H-CF$_3$** as a yellow solid (0.24 g, 36%). ^{1}H NMR (400 MHz, CD_2Cl_2): δ = 7.37-7.58 (m, 16 H), 7.65 (t, *J* = 7.8 Hz, 2 H), 8.13-8.20 (m, 5 H), 8.25 (d, *J* = 7.6 Hz, 2 H); ^{19}F NMR (100 MHz, CD_2Cl_2): δ = -59.20 (s, 3 F); ^{13}C NMR (100 MHz, CD_2Cl_2): δ = 84.2, 109.6, 109.9, 110.0, 110.5, 112.3, 117.0, 120.7, 121.3, 121.5, 121.5, 121.7, 121.9, 122.1, 122.2, 122.4, 122.8, 123.5, 124.6, 124.8, 125.2, 126.2, 127.3, 127.4, 127.5, 130.8, 131.1, 133.5, 139.9, 142.3, 143.8, 144.6, 147.3; HRMS (FAB$^+$, m/z) calcd. for $C_{44}H_{25}F_3N_4$ 666.2031, found 666.2026.

Synthesis of 2,4,6-tri(9*H*-carbazol-9-yl)-5-(trifluoromethyl)isophthalonitrile (3CzIPN-CF$_3$).

Compound **4** (1.80 g, 2.0 mmol), $Pd(PPh_3)_4$ (0.924 g, 0.8 mmol), $Zn(CN)_2$ (0.33 g, 2.8 mmol) and stir bar were mixed in 25 mL two-neck bottle. Under argon atmosphere, 6 mL NMP was added. The reaction was heated at 100 ^{o}C for 3 hr. After cooling to room temperature, the reaction was directly filtered through celite then washed with dichloromethane and concentrated to give the crude product which was then purified by column chromatography (SiO_2, CH_2Cl_2/ Hexane = 1/1) to provide **3CzIPN-CF$_3$** as an orange powder (0.635 g, 46%). ^{1}H NMR (400 MHz, CD_2Cl_2): δ = 7.34 (d, *J* = 8.0 Hz, 6 H), 7.43-7.49 (m, 6 H), 7.57 (t, *J* = 8.4 Hz, 2 H), 7.64 (t, *J* = 7.8 Hz, 4 H), 8.18 (d, *J* = 7.6 Hz, 2 H), 8.23 (d, *J* = 7.6 Hz, 4 H); ^{19}F NMR (100 MHz, CD_2Cl_2): δ = -59.56 (s, 3 F); ^{13}C NMR (100 MHz, CD_2Cl_2): δ = 109.8, 110.4, 110.9, 120.5, 121.7, 121.8, 122.7, 123.5, 125.1, 125.4, 127.5, 127.7, 139.6, 141.8, 147.4, 149.8; HRMS (FAB$^+$, m/z) calcd. for $C_{45}H_{24}F_3N_5$ 691.1984, found 691.1978.

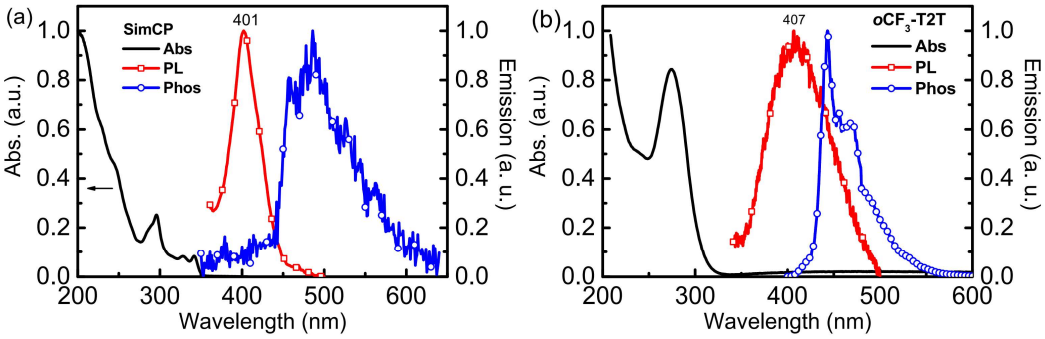

Figure S1. UV-vis absorption, PL, and low-temperature phosphorescence (Phos) of (a) SimCP and (b) *o*CF_3-T2T in neat films.

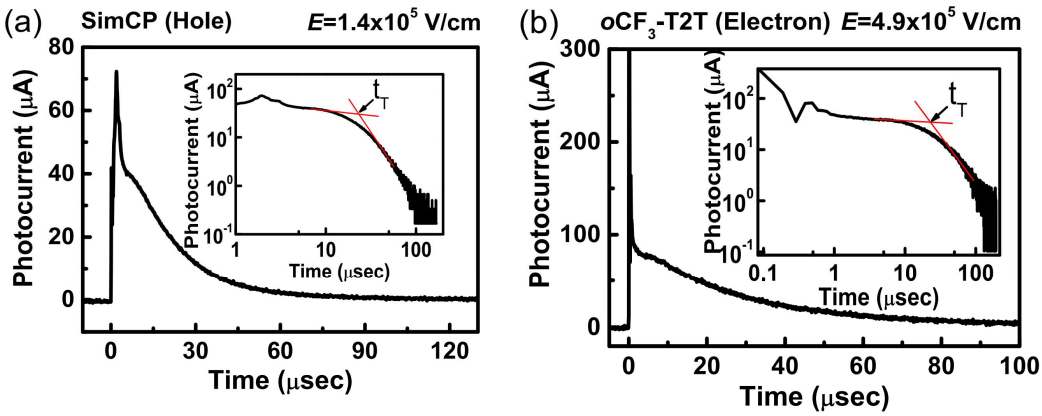

Figure S2. Representative TOF transient photocurrent signals for (a) holes of SimCP at $E = 1.4 \times 10^5$ V cm^{-1}; (b) electrons of *o*CF_3-T2T at $E = 4.9 \times 10^5$ V cm^{-1} and insets are the double logarithmic plots.

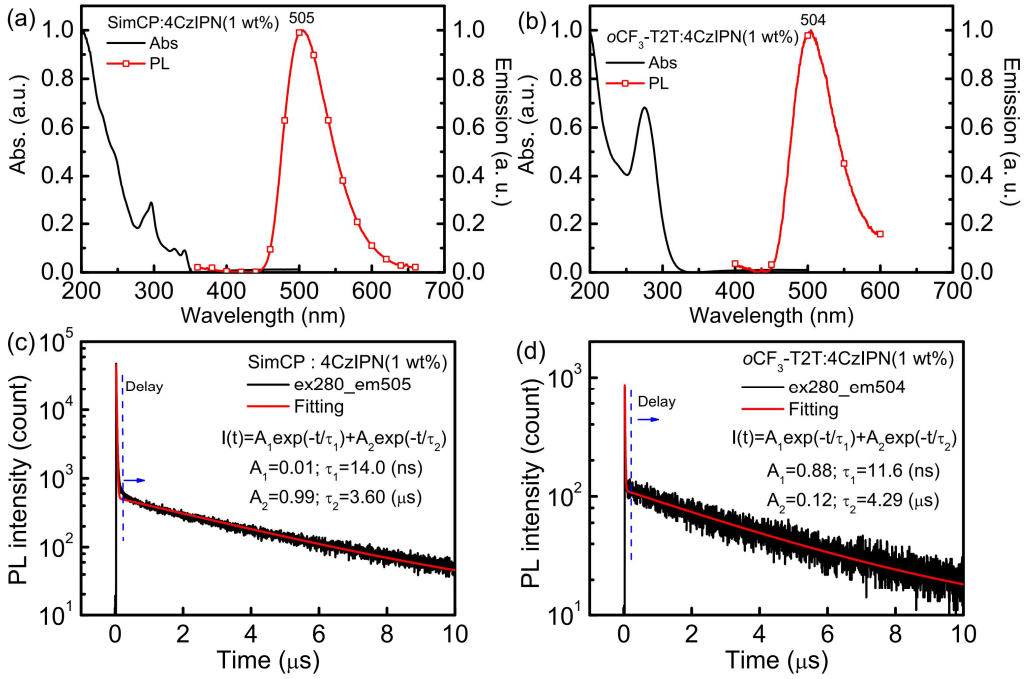

Figure S3. (a)(b)The absorption and PL spectra, (c)(d) transient PL decays of 1 wt% 4CzIPN doped in SimCP and oCF_3-T2T, respectively.

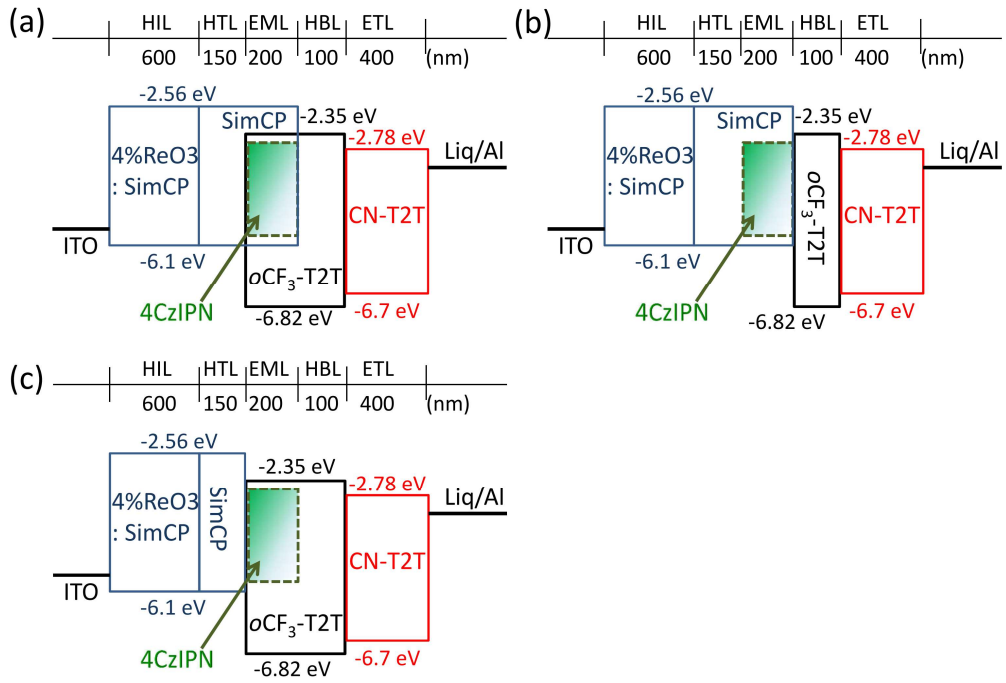

Scheme S1. Schematic OLED structure with 4CzIPN doped in (a) SimCP:oCF_3-T2T, (b) SimCP and (c)oCF_3-T2T as EML.

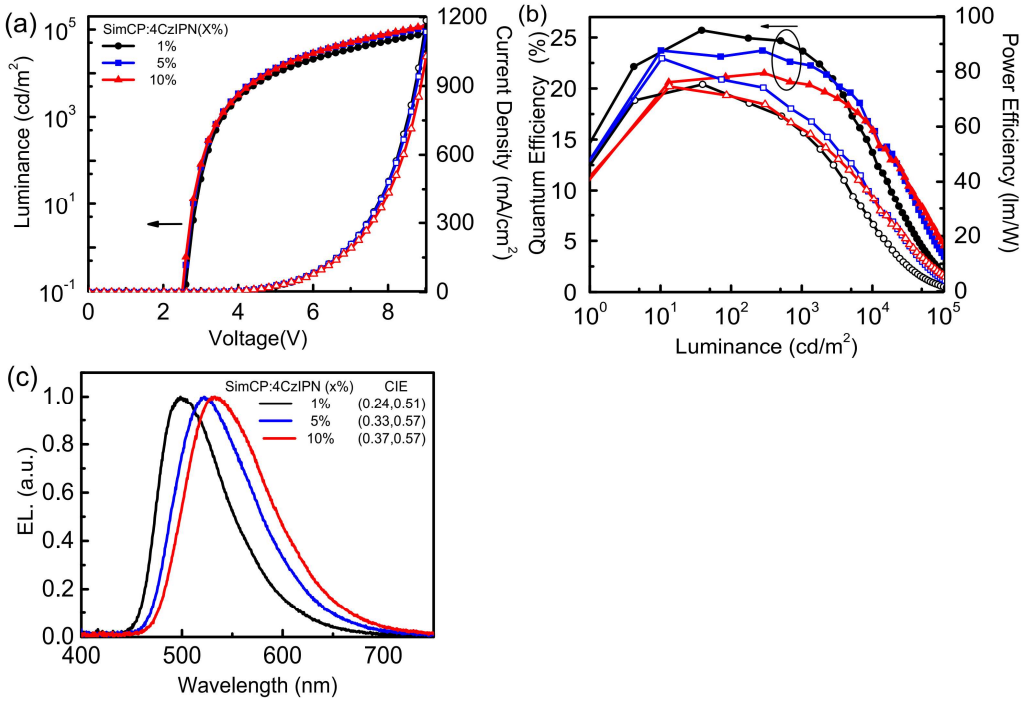

Figure S4. (a) *J-V-L* characteristics, (b) *EQE–PE–L* characteristics, and (c) normalized EL spectra for SimCP: x wt% 4CzIPN devices.

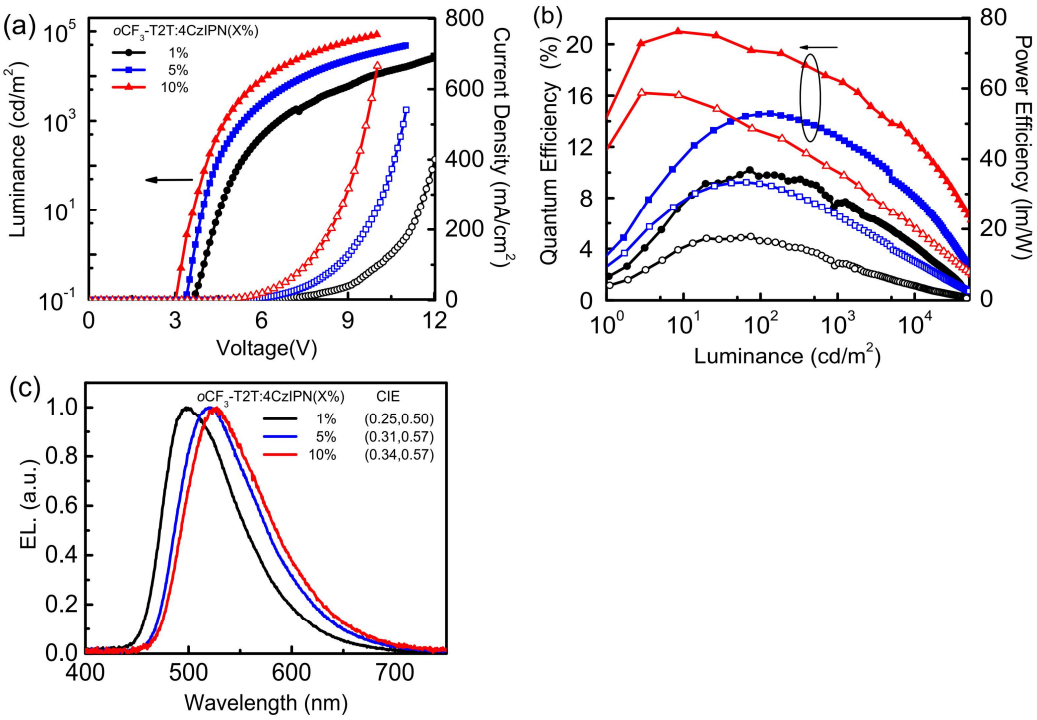

Figure S5. (a) *J-V-L* characteristics, (b) *EQE–PE–L* characteristics, (c) normalized EL spectra and (d) emission for *o*CF_3-T2T: x wt% 4CzIPN devices.

Table S1. The PLQY and horizontal dipole ratio of emitters, as well as experimentally obtained EQEs of the devices.[2]

host	dopant	PLQY (%)	[a] $\Theta_{//}$ (%)	[b] $Ø_{out}$ (%)	PLQY *$Ø_{out}$ (%)	EQE_{max} (%)
SimCP:*o*CF_3-T2T	10 wt% 4CzIPN	83	80	32.8	27.2	25.2
SimCP		81	72	30.1	24.3	21.3
oCF_3-T2T		78	71	29.3	22.8	20.1
SimCP: *o*CF_3-T2T	1 wt% 4CzIPN	82	83	34.5	28.3	26.1
	1 wt% **4CzIPN-CF_3**	77	80	32.9	25.3	23.1
	1 wt% **3CzIPN-H-CF_3**	63	72	30.1	18.9	16.5
	1 wt% **3CzIPN-CF_3**	56	73	31.2	17.7	16.4

[a] Horizontal dipole ratio. [b] Calculated optical outcoupling efficiency by Setfos Integration Module software package (FLUXIM AGT).

[2] Lin, T.-A.; Chatterjee, T.; Tsai, W.-L.; Lee, W.-K.; Wu, M.-J.; Jiao, M.; Pan, K.-C.; Yi, C.-L.; Chung, C.-L.; Wong, K.-T.; Wu, C.-C. Sky-Blue Organic Light Emitting Diode with 37% External Quantum Efficiency Using Thermally Activated Delayed Fluorescence from Spiroacridine-Triazine Hybrid. *Adv. Mater.* **2016**, *28*, 6976-6983.

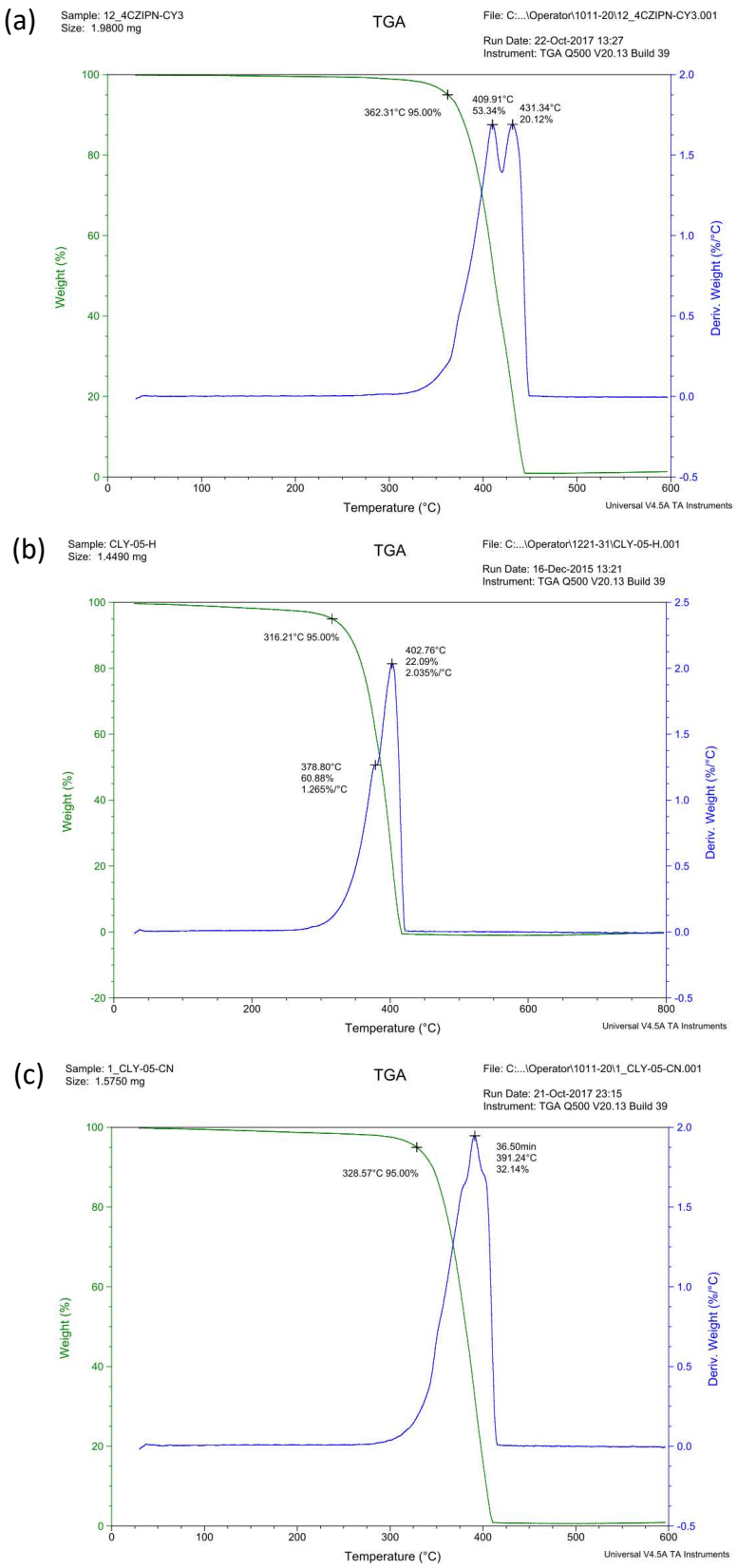

Figure S6. The thermogravimetric analysis (TGA) of (a) **4CzIPN-CF$_3$**, (b) **3CzIPN-H-CF$_3$** and (c) **3CzIPN-CF$_3$**.

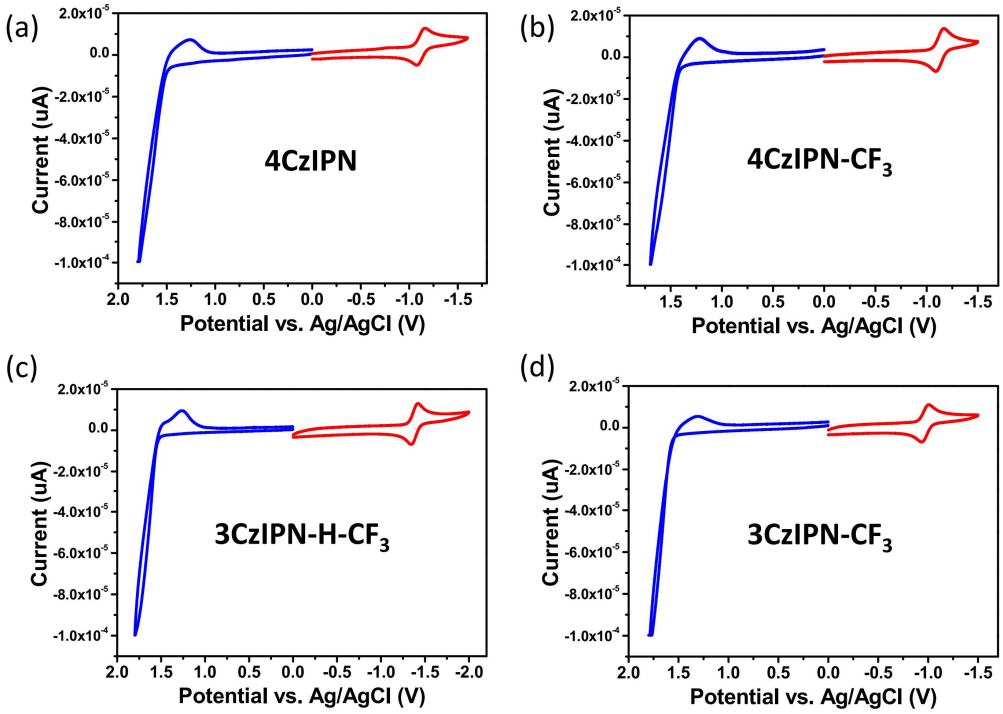

Figure S7. Cyclic voltammetry curves of (a) **4CzIPN**, (b) **4CzIPN-CF$_3$**, (c) **3CzIPN-H-CF$_3$** and (d) **3CzIPN-CF$_3$**.

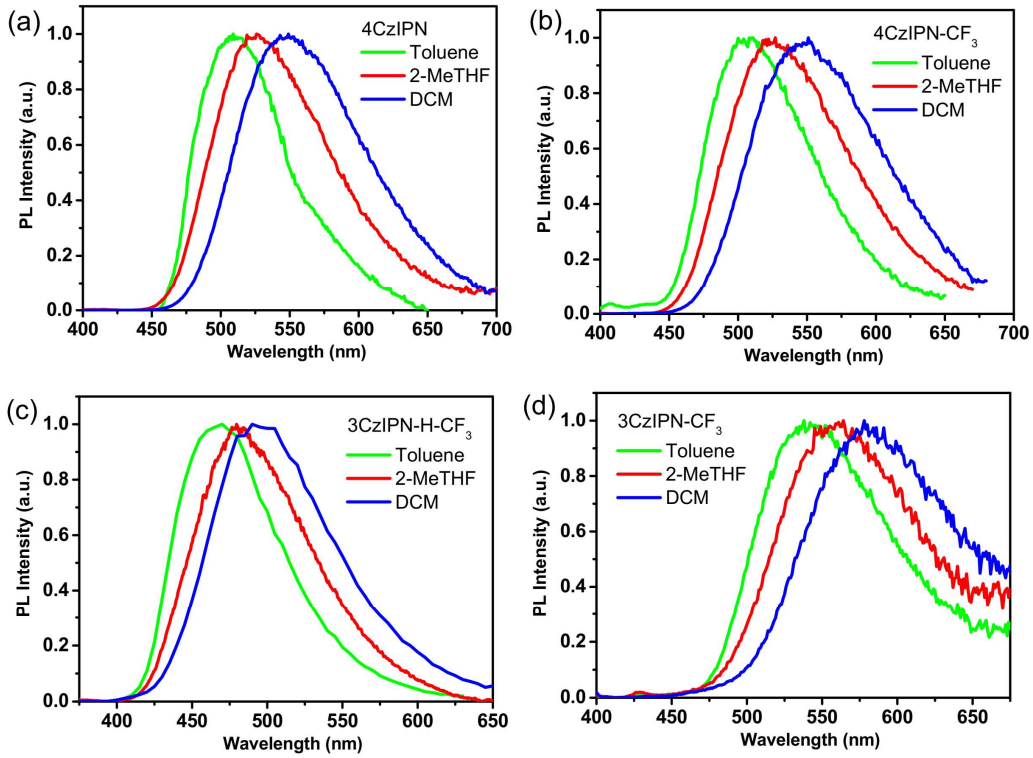

Figure S8. Solvatochromic photoluminescence spectra of (a) **4CzIPN**, (b) **4CzIPN-CF$_3$**, (c) **3CzIPN-H-CF$_3$** and (d) **3CzIPN-CF$_3$**.

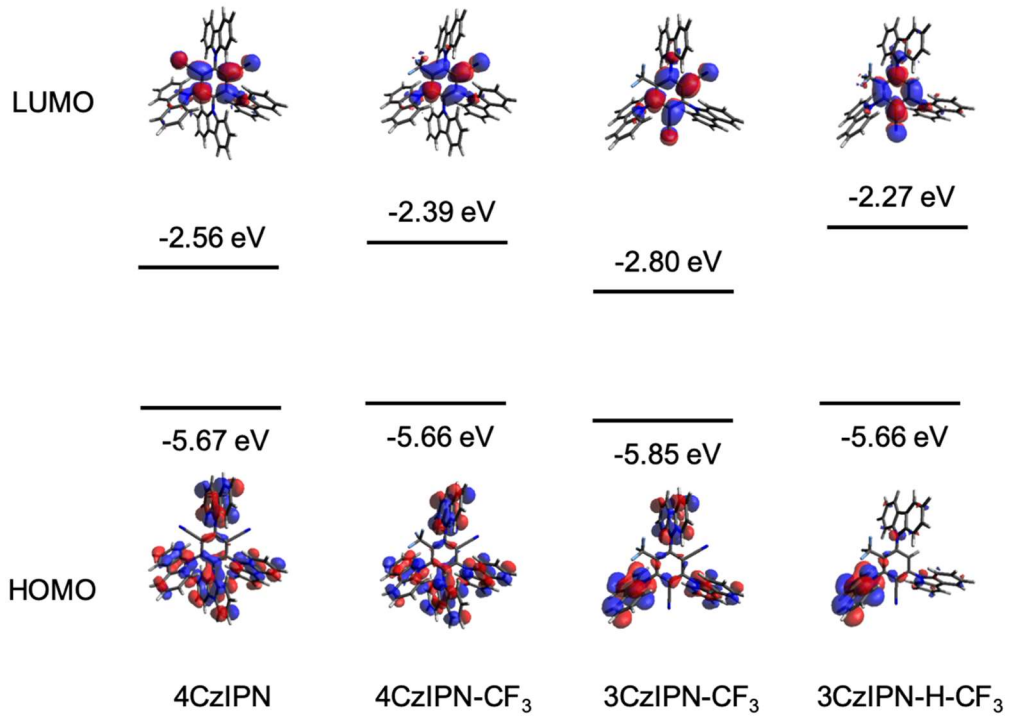

Figure S9. Calculated HOMO, LUMO and energy levels of 4CzIPN, **4CzIPN-CF₃**, **3CzIPN-H-CF₃** and **3CzIPN-CF₃**

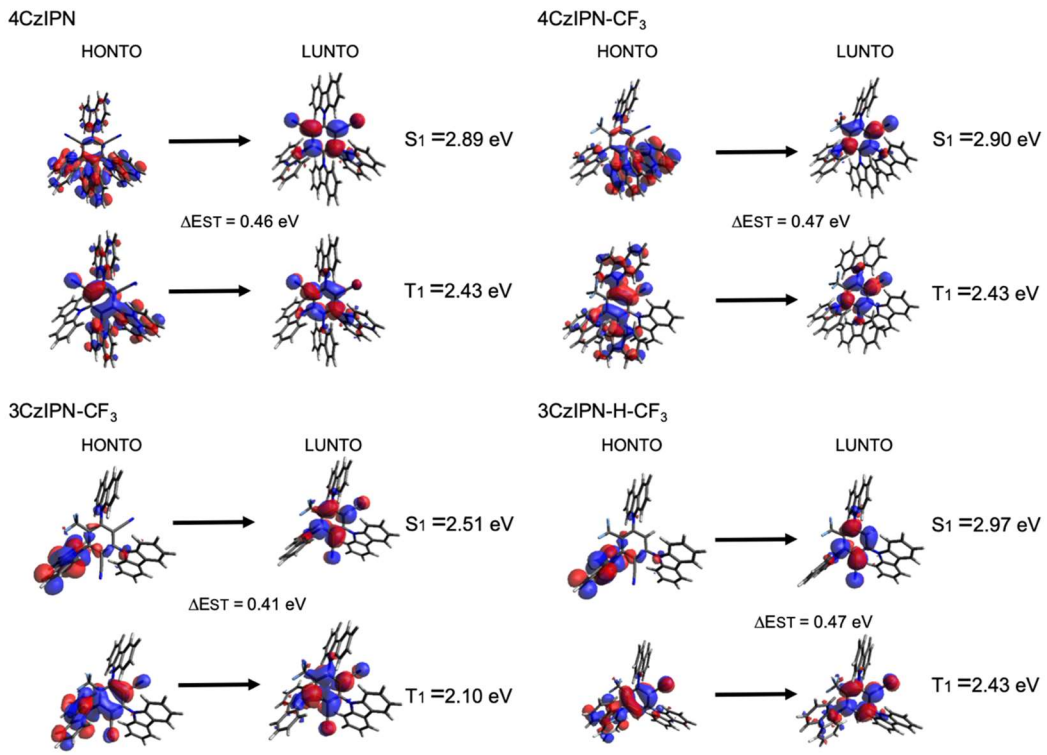

Figure S10. Calculated Nature Transition Orbital (NTO) for both $S_0 \rightarrow S_1$ and $S_0 \rightarrow T_1$ excitations based on the optimized S_1 and T_1 geometries of **4CzIPN, 4CzIPN-CF₃**, **3CzIPN-H-CF₃** and **3CzIPN-CF₃**

Table S2. Theoretically calculated data with DFT/TD-TFT method

	HOMO (eV)	LUMO (eV)	λ S_1 (nm)	S_1 (eV)	T_1 (eV)	ΔE_{ST} (eV)
4CzIPN	-5.67	-2.56	430	2.89	2.43	0.46
4CzIPN-CF_3	-5.66	-2.39	427	2.90	2.43	0.47
3CzIPN-CF_3	-5.85	-2.80	494	2.51	2.10	0.41
3CzIPN-H-C_{F3}	-5.66	-2.27	418	2.97	2.50	0.47

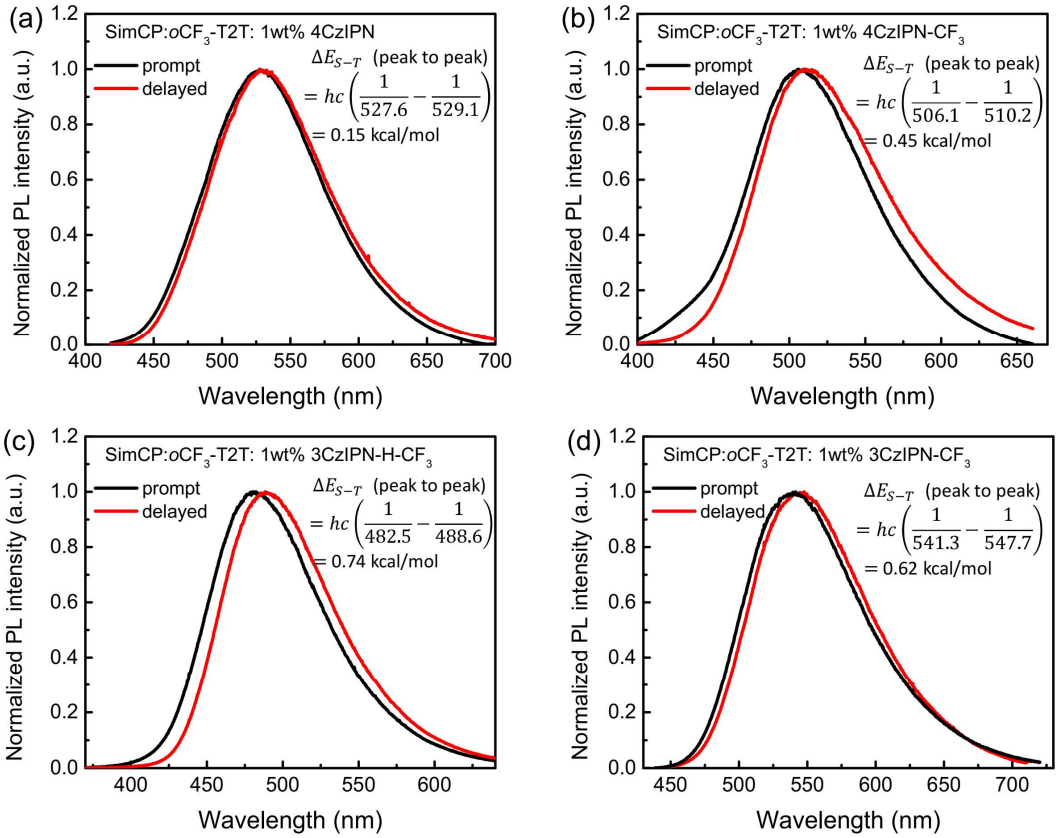

Figure S11. Time-resolved PL spectra of the films by SimCP:*o*CF_3-T2T doped with 1 wt% (a) 4CzIPN, (b) **4CzIPN-CF_3** (c) **3CzIPN-H-CF_3** and (d) **3CzIPN- CF_3** at 300 K. Prompt (black line: delay = 0 ns, gate width 100 ns) and delayed 20 μs (red line: gate width = 10 μs) components of the PL spectra.

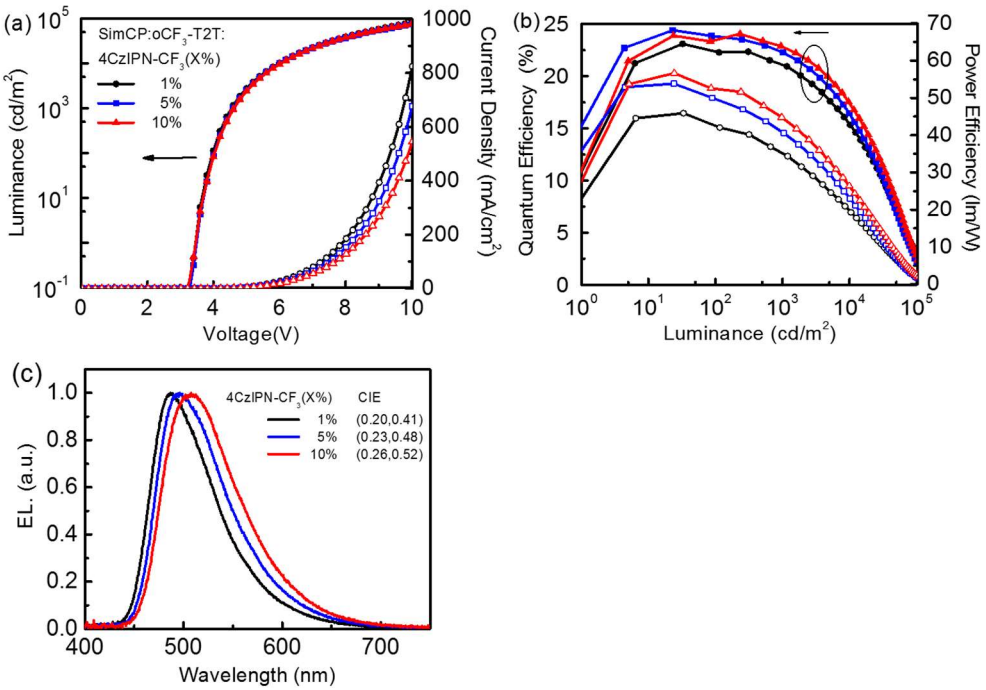

Figure S12. (a) *J-V-L* characteristics, (b) *EQE–PE–L* characteristics, and (c) normalized EL

spectra for SimCP:*o*CF_3-T2T: x wt% **4CzIPN-CF_3** devices.

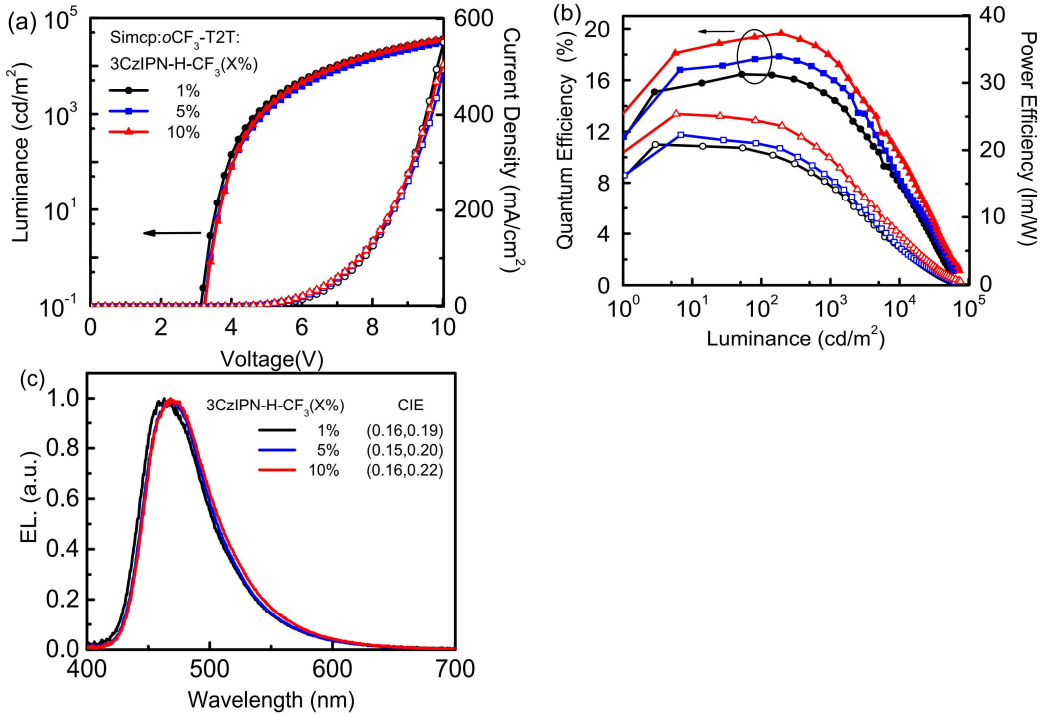

Figure S13. (a) *J-V-L* characteristics, (b) *EQE–PE–L* characteristics, and (c) normalized EL spectra for SimCP:*o*CF_3-T2T: x wt% **3CzIPN-H-CF_3** devices.

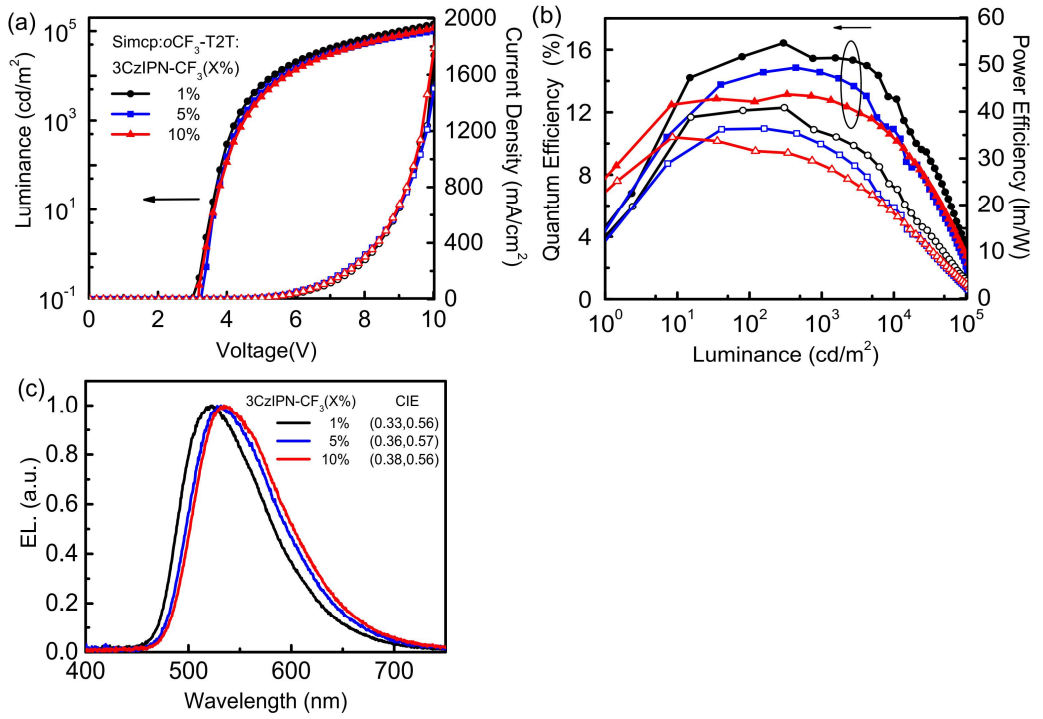

Figure S14. (a) *J-V-L* characteristics, (b) *EQE–PE–L* characteristics, and (c) normalized EL spectra for SimCP:*o*CF_3-T2T: x wt% **3CzIPN-CF_3** devices.

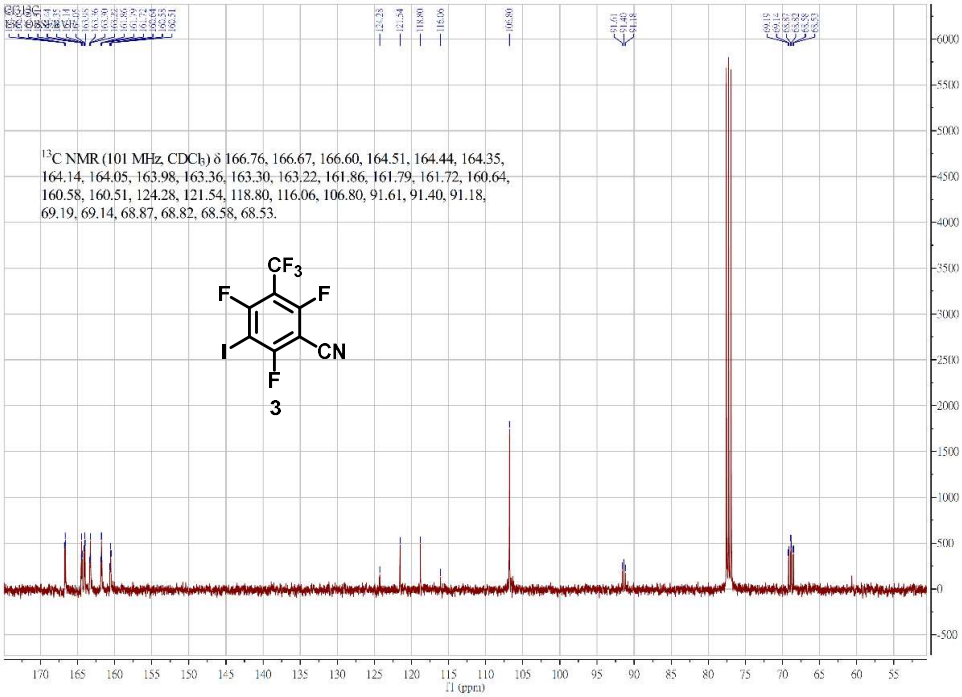

Figure S15. The ^{13}C NMR of **3**.

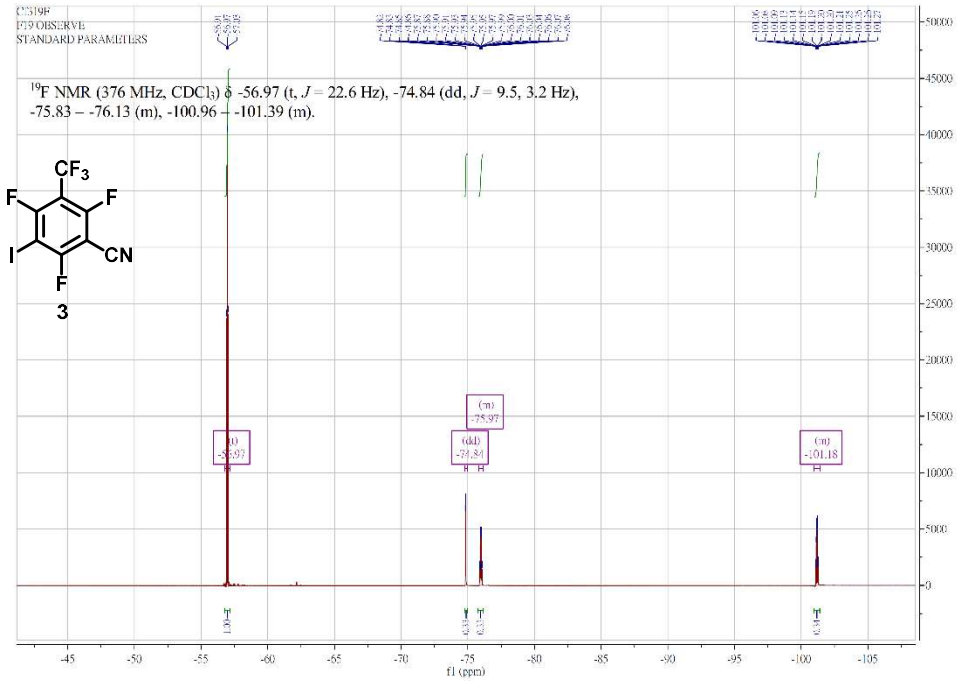

Figure S16. The ^{19}F NMR of **3**.

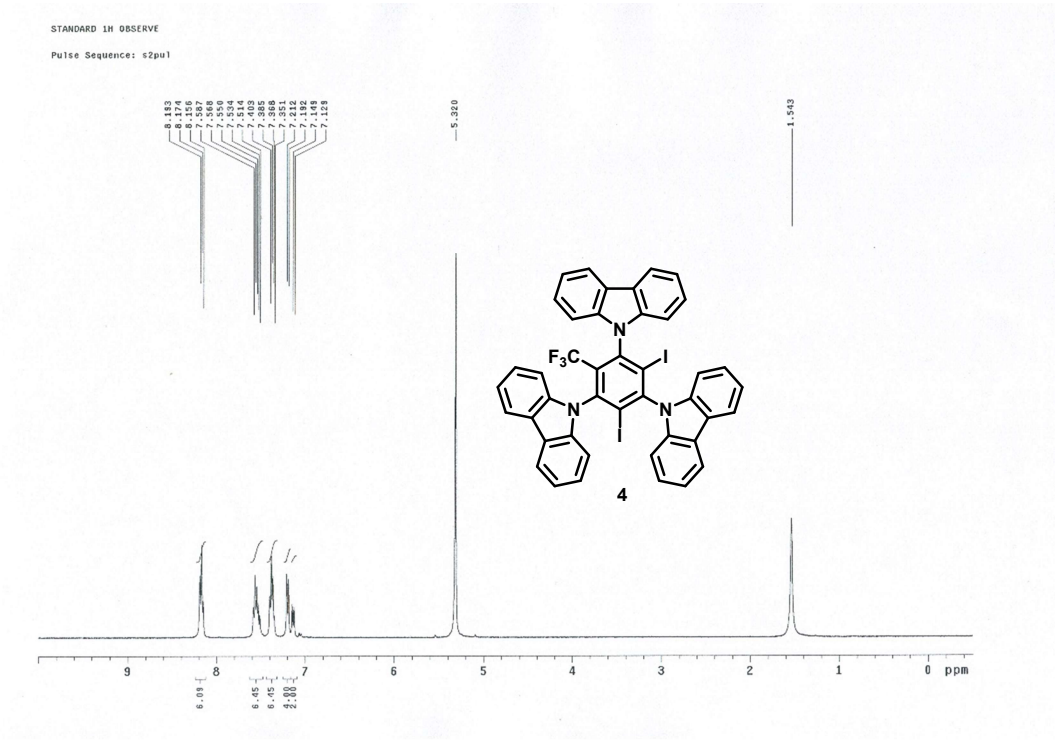

Figure S17. The ^{1}H NMR of **4**.

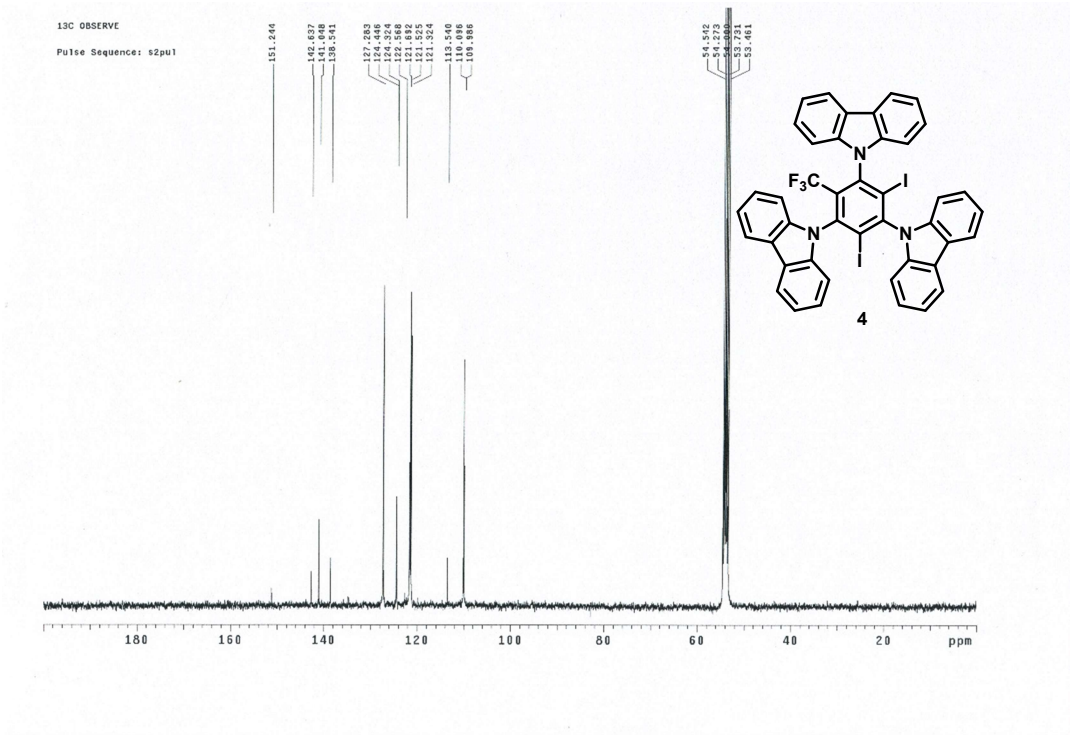

Figure S18. The ^{13}C NMR of **4**.

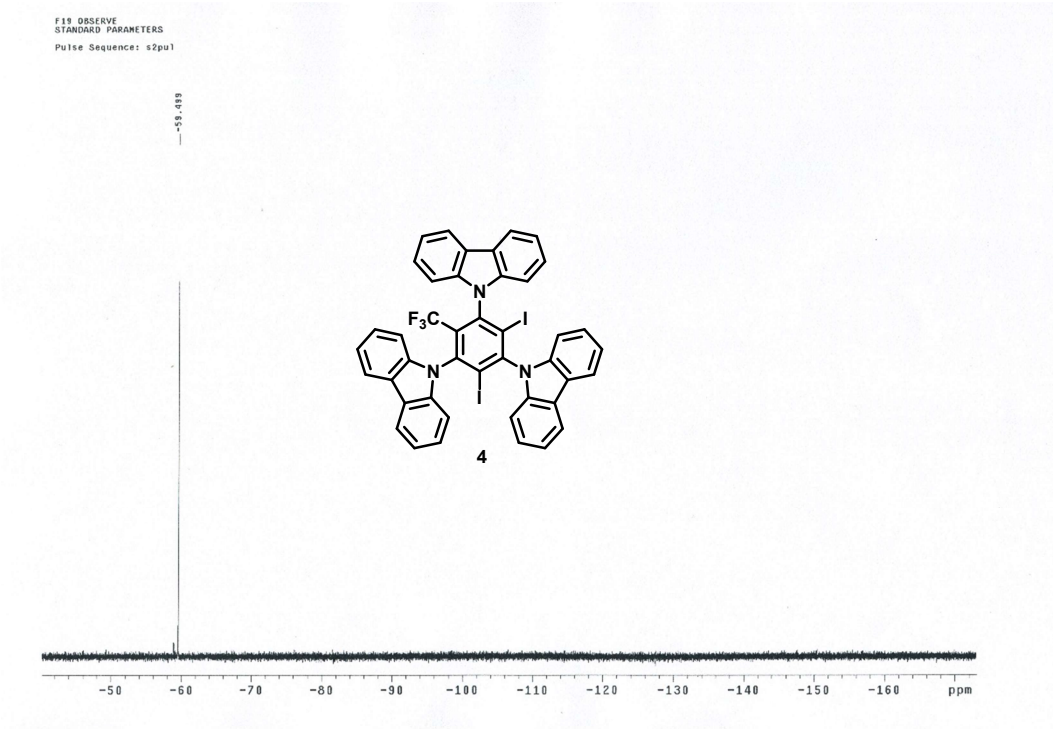

Figure S19. The ^{19}F NMR of **4**.

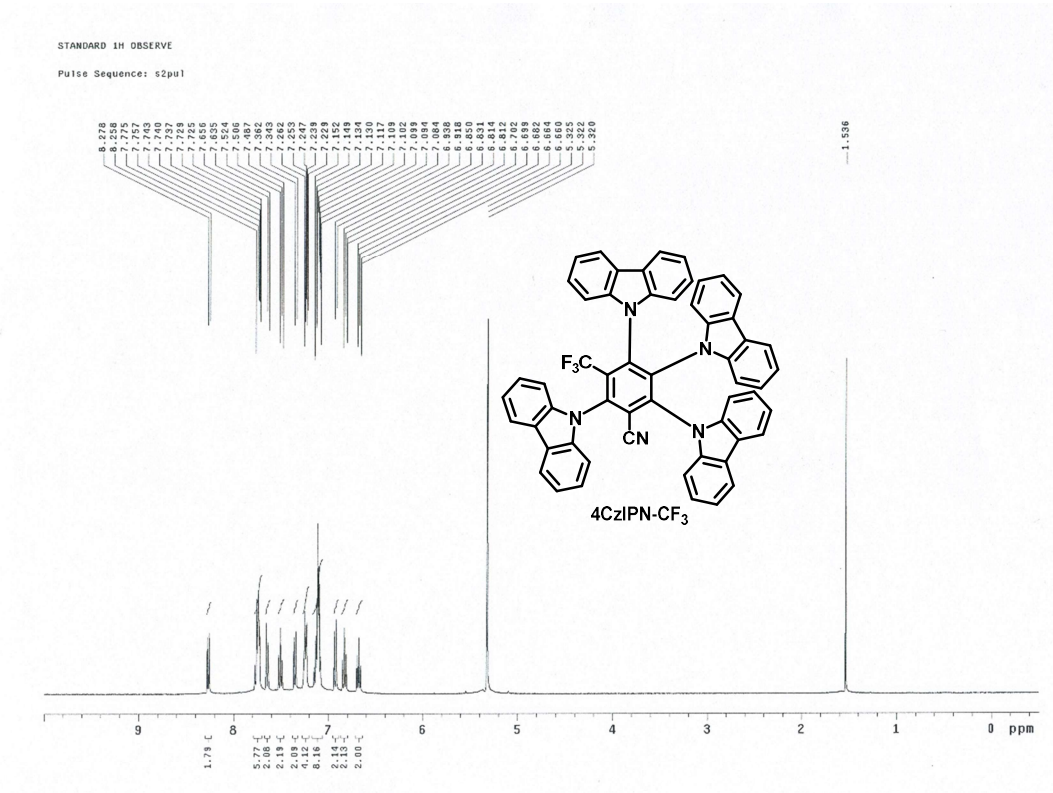

Figure S20. The ^{1}H NMR of **4CzIPN-CF$_3$**.

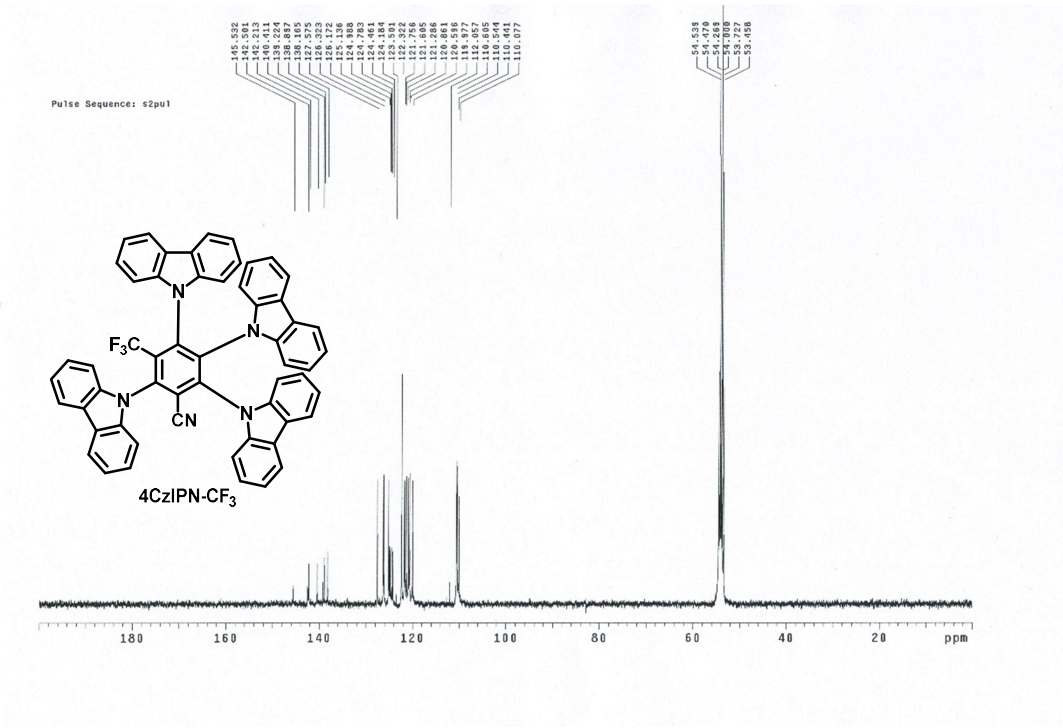

Figure S21. The ^{13}C NMR of **4CzIPN-CF₃**.

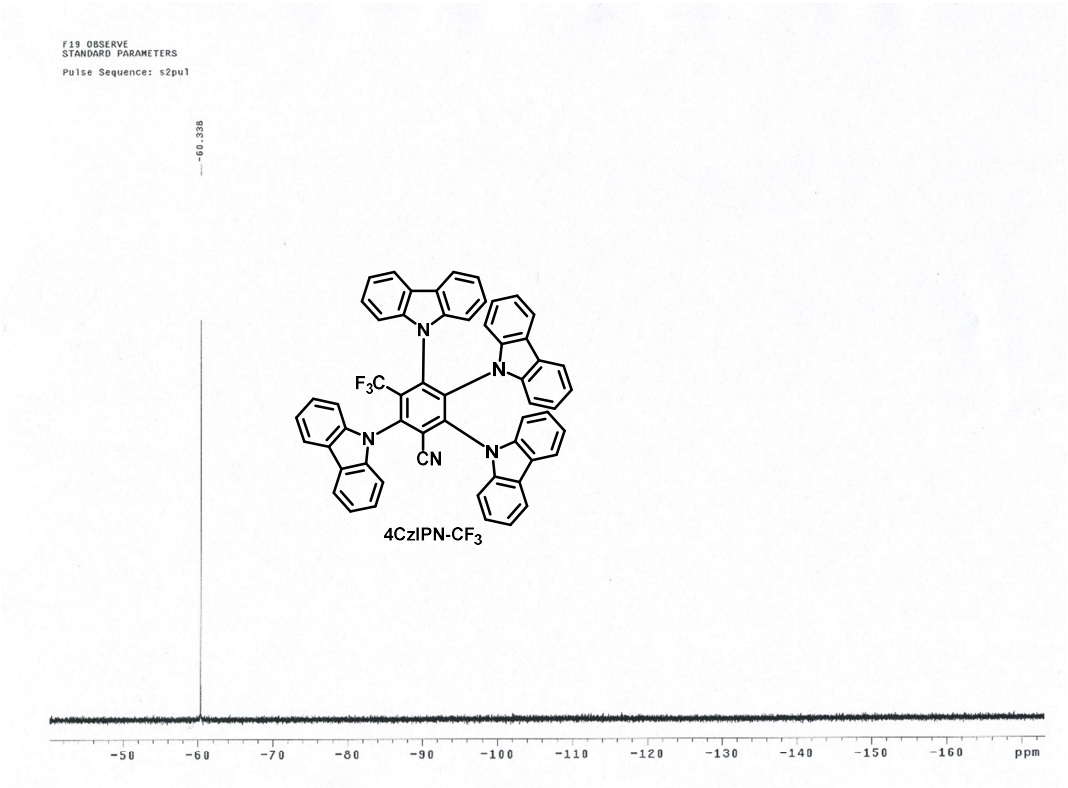

Figure S22. The ^{19}F NMR of **4CzIPN-CF₃**.

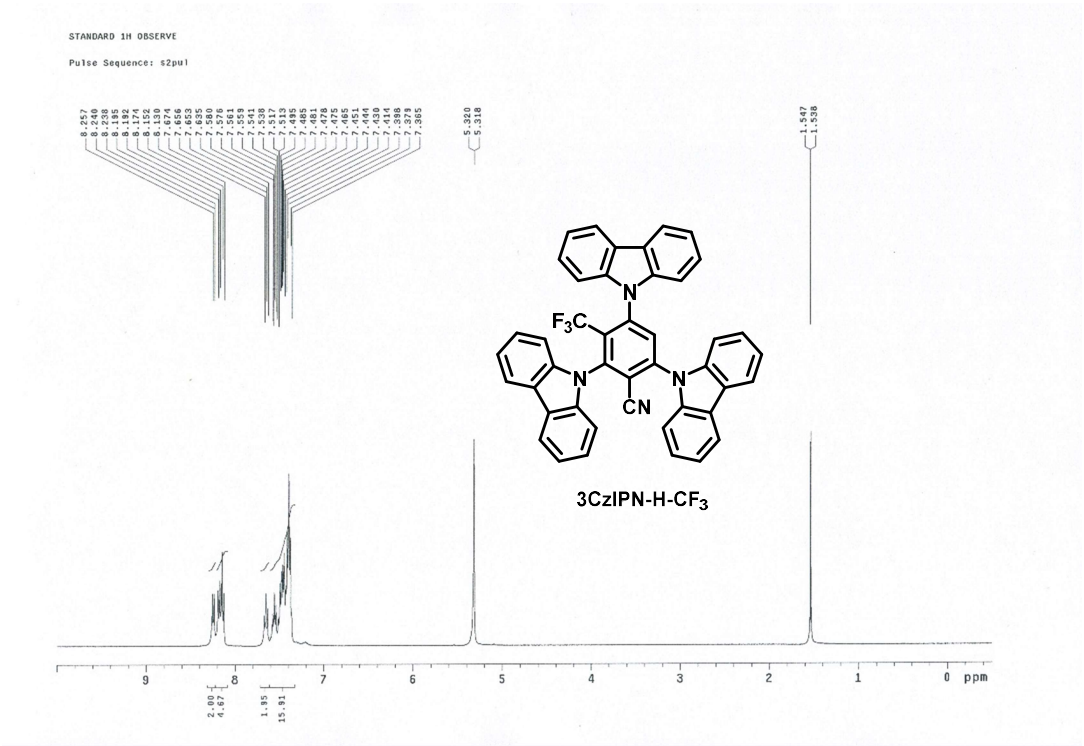

Figure S23. The ^{1}H NMR of **3CzIPN-H-CF$_3$**.

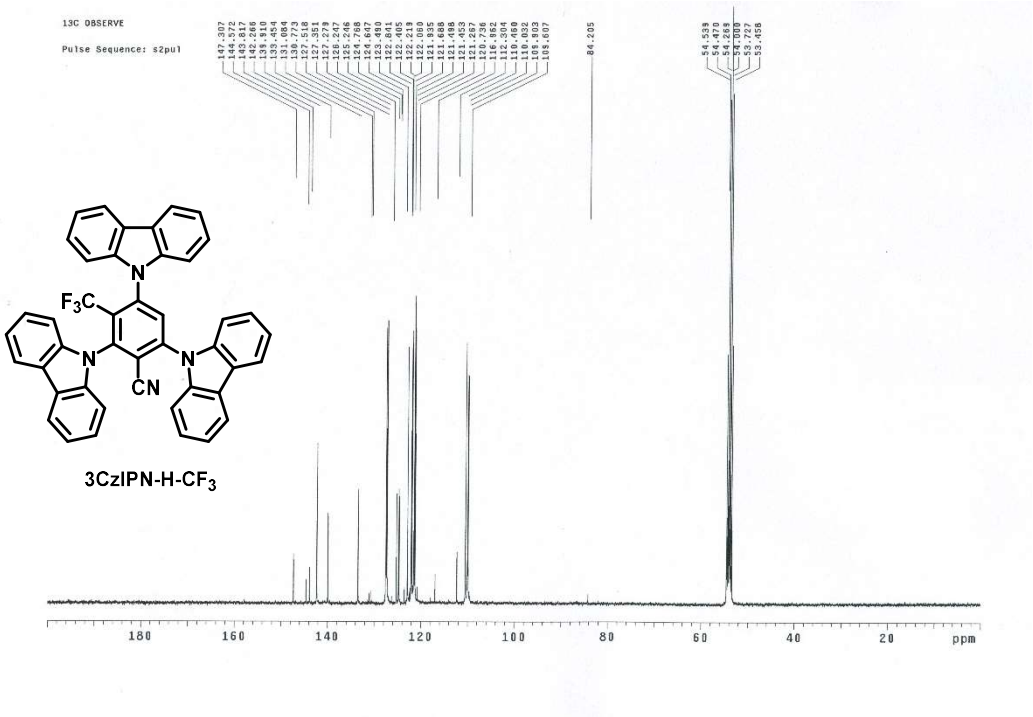

Figure S24. The ^{13}C NMR of **3CzIPN-H-CF$_3$**.

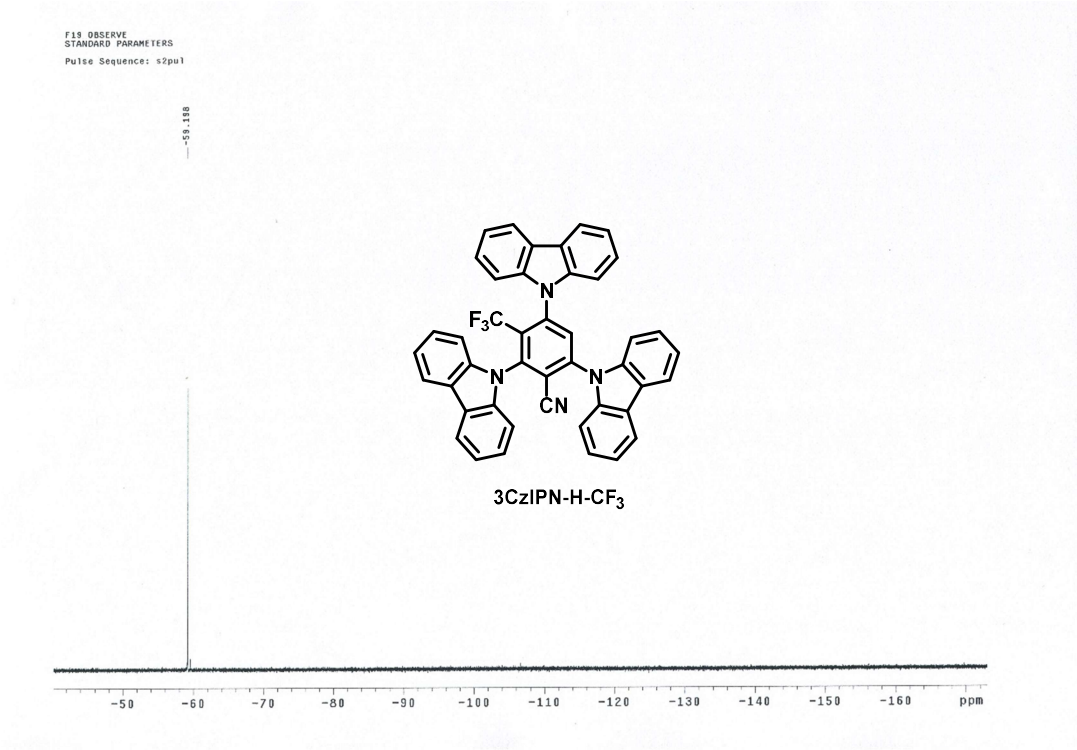

Figure S25. The ^{19}F NMR of **3CzIPN-H-CF$_3$**.

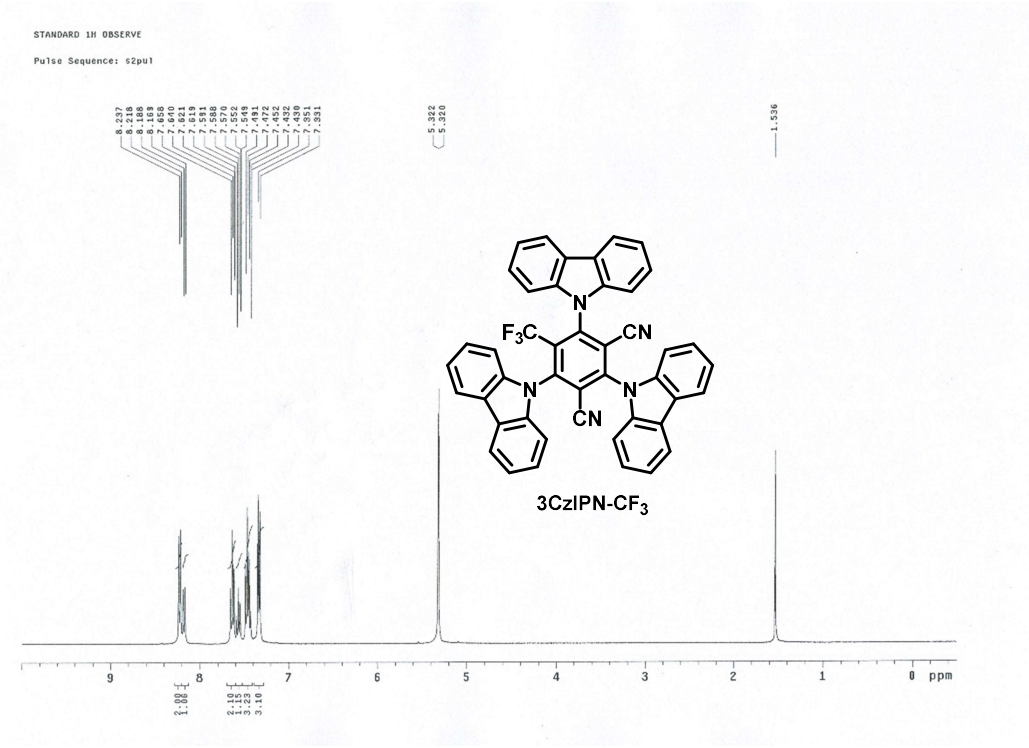

Figure S26. The ^{1}H NMR of **3CzIPN-CF$_3$**.

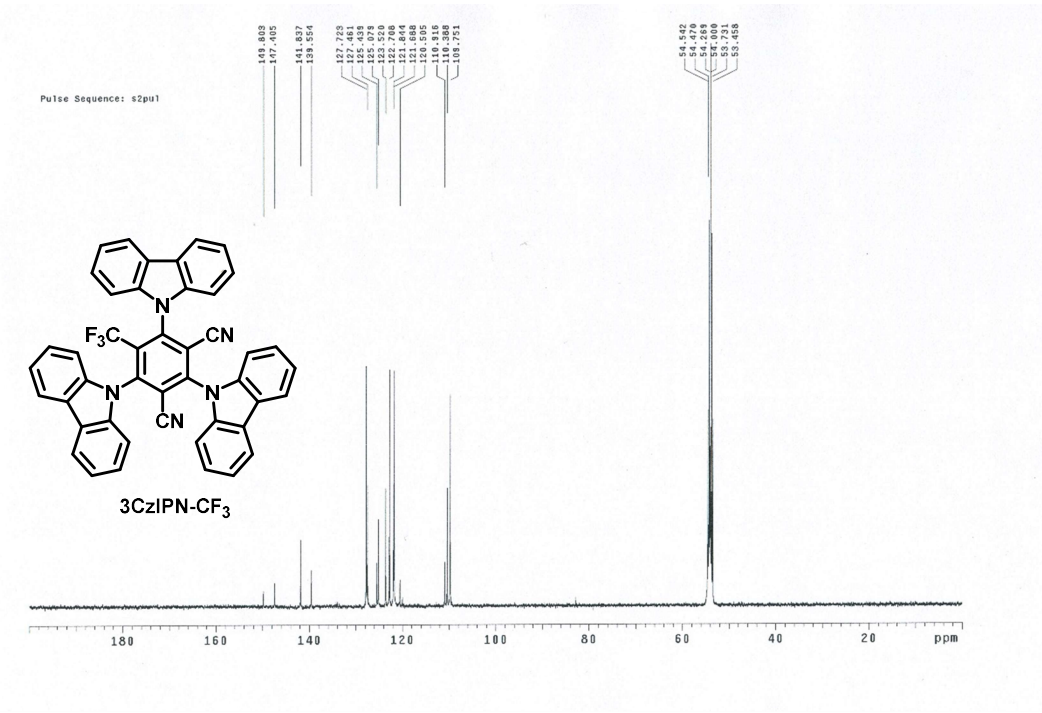

Figure S27. The ^{13}C NMR of **3CzIPN-CF$_3$**.

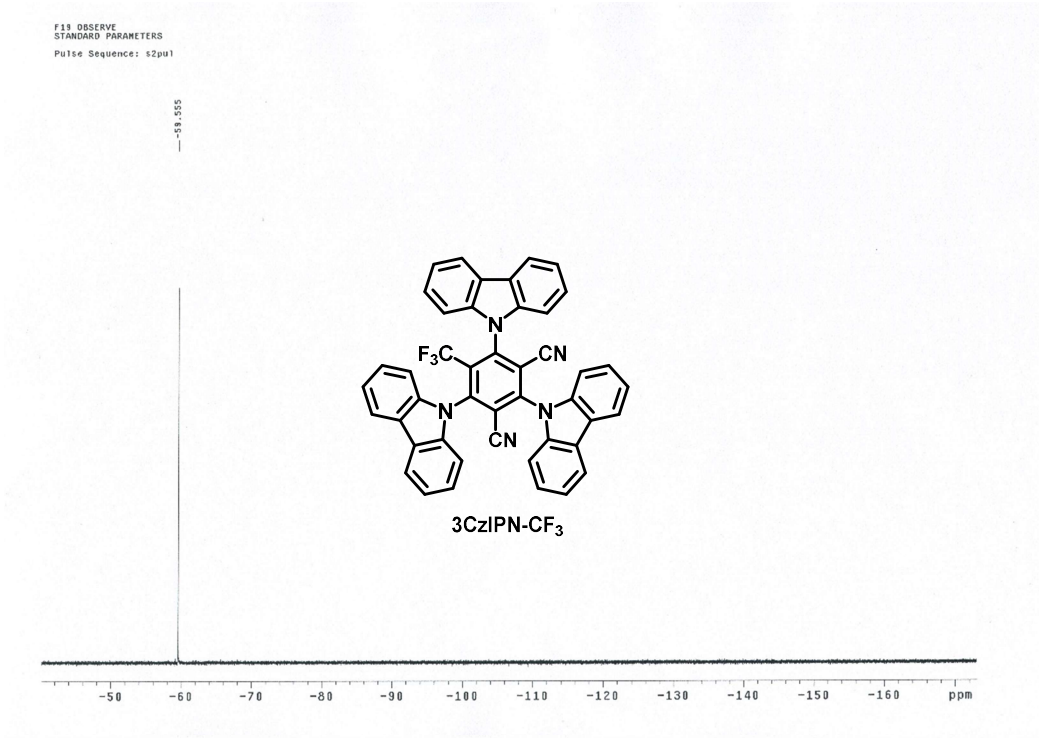

Figure S28. The ^{19}F NMR of **3CzIPN-CF$_3$**.